Biophysical Letter

Dynamics of Cell Area and Force during Spreading

Yifat Brill-Karniely,[1] Noam Nisenholz,[1] Kavitha Rajendran,[2] Quynh Dang,[2] Ramaswamy Krishnan,[2] and Assaf Zemel[1,*]

[1]Institute of Dental Sciences and Fritz Haber Center for Molecular Dynamics, Hebrew University of Jerusalem, Israel; and [2]Center for Vascular Biology Research, Beth Israel Deaconess Medical Center, Boston, Massachusetts

ABSTRACT Experiments on human pulmonary artery endothelial cells are presented to show that cell area and the force exerted on a substrate increase simultaneously, but with different rates during spreading; rapid-force increase systematically occurred several minutes past initial spreading. We examine this theoretically and present three complementary mechanisms that may accompany the development of lamellar stress during spreading and underlie the observed behavior. These include: 1), the dynamics of cytoskeleton assembly at the cell basis; 2), the strengthening of acto-myosin forces in response to the generated lamellar stresses; and 3), the passive strain-stiffening of the cytoskeleton.

Received for publication 3 July 2014 and in final form 9 October 2014.

*Correspondence: assaf.zemel@ekmd.huji.ac.il

Yifat Brill-Karniely's present address is Institute for Drug Research, The School of Pharmacy, The Hebrew University of Jerusalem, Israel

When cells spread on a substrate, a thin lamella compartment develops at the cell basis and progressively extends the cell projected area (1). At the lamella front, lamellipodia protrusions are formed from a highly branched and dense actin network that polymerizes against the cell membrane and pushes the front of the cell forward (2). Supported by cell-substrate friction, these molecularly complex protrusions act as motor units that drive cell spreading and locomotion (2).

Experiments on endothelial cells are presented (Fig. 1) to demonstrate that the increase in cell projected area occurs concurrently with a rise in the exerted force on the substrate. Interestingly, we systematically find that the increase in cellular force is moderate at early times and that the rapid development of force occurs a few minutes past initial spreading; similar behavior has been reported for fibroblasts on a pillared surface (3). To explain these dynamics, we suggest an elastic picture whereby the motor activity of the cell front elastically stretches the lamellar cytoskeleton, and three mechanisms are examined that may underlie the observed delay in force generation. This elastic picture is motivated by previous studies that consistently show that cell area and force are both monotonically increasing functions of substrate rigidity (4,5), and that the total steady-state force exerted onto the substrate increases with the projected cell area (Reinhart-King et al. (4), and see Fig. S3 in the Supporting Material).

Based on these evidences, we have recently developed an elastic theory of cell-spreading dynamics (5). The theory successfully accounts for a variety of spreading characteristics such as the concurrent increase in the actin retrograde flow with the slowing-down of spreading (1) and the dependence of cell-spreading dynamics on substrate rigidity and surface ligand density. We have also shown that the nonlinear elasticity of the cytoskeleton can explain the observed delay in force production. Here we present two alternative and complementary mechanisms that may underlie this behavior; for yet another mechanism, see Fouchard et al. (6).

Our starting point is the linear theory described in detail in Nisenholz et al. (5). Accordingly, the lamella is modeled as a homogeneous and isotropic elastic disk of thickness h and radius R, which is actively stretched by propulsion of the cell front-forward (see Fig. S1). The cell adheres to the substrate via multiple (transient) adhesion contacts that typically concentrate in a narrow rim at the cell front (2). The radial velocity of the cell front is dictated by two oppositely oriented motions:

$$\dot{R}(t) = v_{\mathrm{pol}} - v_F(t). \quad (1)$$

Here, v_{pol} is the constant radial actin polymerization speed at the cell front (1,5), and $v_F(t)$ is the increasing retrograde flow of the lamellar network due to the rise in cellular tension (1,2). Myosin activity is implicitly accounted for in its contribution to the effective elasticity of the lamella

Editor: Christopher Yip.

http://dx.doi.org/10.1016/j.bpj.2014.10.049

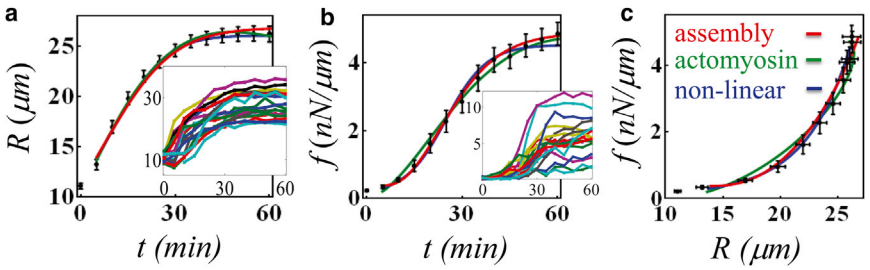

FIGURE 1 Evolution of mean ($n = 47$) cell radius (*a*) and force (*b*); (*solid lines*) theoretical fits to the three models; (*insets*) respective dynamics of individual cells. (*c*) Mean force, $f(t)$, versus temporal cell radius $R(t)$. See fitting parameters and additional information in the Supporting Material. To see this figure in color, go online.

network. The forward motion of the lamellipodium stretches the cytoskeleton, and as a result a visco-elastic force is developed in the lamella:

$$f/h = 2\kappa_c\,(R - R_0)/R_0 + \xi_c\, d(R/R_0)/dt. \qquad (2)$$

Here $f = F/(2\pi R)$ is the radial force per unit length; F is the total cell force; κ_c is the effective, long-term, area-expansion modulus of the lamella; ξ_c is the effective viscosity coefficient; and R_0 is an associated rest length of this elastic continuum from which elastic forces are dictated.

Assuming linear (force-independent) cell-substrate friction coefficient, ξ_s (5), the retrograde flow, $v_F(t)$, may be related to the force $f(t)$ via $v_F(t) = f(t)/\xi_s$. Combining this with Eq. 1 results in the linear force-velocity relation

$$f = f_{ss}\left(1 - \dot{R}/v_{pol}\right), \qquad (3)$$

where $f_{ss} = \xi_s v_{pol}$ is the steady-state force, which depends on substrate rigidity via ξ_s's dependence on rigidity (5,7). Equating 3 and 2 and assuming R_0 to be fixed, results in a linear differential equation for $R(t)$ and $f(t)$, with the simple solution $R(t) \sim f(t) \sim 1 - \exp(-t/\tau)$, where $\tau = [\xi_c + R_0\xi_s/h]/(2\kappa_c)$. We now describe three possible extensions of this basic model to explain the interesting (nonlinear) coupling in the behavior of $R(t)$ and $f(t)$; all three mechanisms are believed to contribute simultaneously (see Fig. S1), but for clarity, we treat them separately, as follows.

I: dynamics of lamellar network assembly

Our approach to this complex reorganization process of the cytoskeleton is based on a simple kinetic scheme in which suspended constituents of the cytoskeleton assemble the semi-two-dimensional lamellar network at the cell basis. This process, which gives rise to a gradual increase in the elastic rest length, R_0, occurs concurrently with cell spreading as observed in experiments (4); the driving force is assumed to be force-independent for simplicity and is reflected in the rate constants of the assembly process. We assume a constraint on the overall mass of cytoskeletal material that may eventually assemble at the cell basis and we denote this mass by M_{tot}. Furthermore, for simplicity, we consider only two forms of this material: either suspended in the cell volume, V, or incorporated in the two-dimensional network at the cell basis. Mass conservation is then given as

$$M_{tot} = c(t)\,V + \rho\,A_0(t), \qquad (4)$$

where $c(t)$ is the total concentration of suspended cytoskeleton material (primarily actin), $A_0(t) = \pi R_0^2$ is the total (elastically relaxed) area of the two-dimensional network, ρ is the surface density of this material, and ρ and V are assumed to be constant. Assuming that the rate of area growth is proportional to both $c(t)$ and the assembled area, $A_0(t)$, we write

$$\dot{A}_0 = \delta c(t) A_0(t), \qquad (5)$$

where δ is the corresponding effective binding rate constant of suspended cytoskeletal fragments to the lamella network. Equations 4 and 5 provide a minimal model for the kinetics of network assembly at the cell basis, and for the variations of the elastically relaxed radius, $R_0(t)$, in particular. Although neglecting many details in this process, the simple model presented suffices us here as a minimal model for examining the consequences of network assembly on the mechanics of spreading. The progressive growth of $R_0(t)$ relaxes the tension being created by the pulling of lamellipodia protrusions at the cell front (see Eq. 2). Consequently, the cell can initially spread with minor increase in force, providing a plausible explanation to the observed delay in force production (Fig. 1). Once the suspended material available for assembly has fully integrated into the network, a second, elastic phase begins where the force rapidly increases with cell area. This behavior explains why we may neglect the force-dependence of the rate constant δ, inasmuch as forces develop mainly after the assembly process is finished. A fit of this model to the experimental data is shown in Fig. 1 (*red curves*). The assembly model also predicts an interesting effect of cell volume on the spreading dynamics, as shown in the Supporting Material (see Fig. S2).

II: strengthening of actomyosin forces in the course of spreading

Whereas in our previous sections myosin activity has only implicitly been accounted for in contributing to the

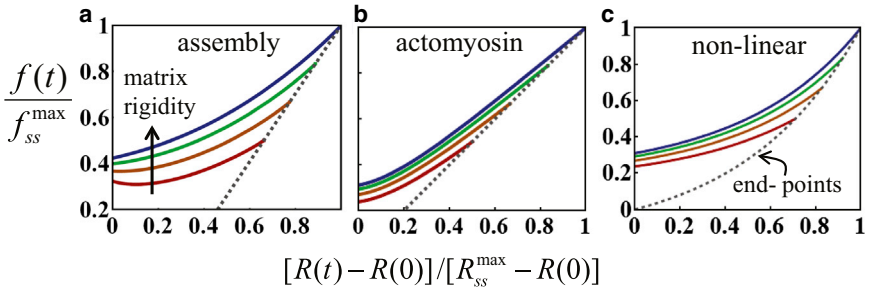

FIGURE 2 Comparison of the (scaled) $f(t)$ versus $R(t)$ plot for the three proposed models (*a–c*). Different curves correspond to different substrate rigidities. Dotted lines mark the steady-state. R_{ss}^{max} and f_{ss}^{max} are the steady-state radius and force for an infinitely rigid substrate, respectively. In all panels we took $\xi_s/\xi_s^{max} = E_m/(E_m + E_c) =$ 0.5 (*red*), 0.67 (*orange*), 0.83 (*green*), and 0.99 (*blue*), where E_m and E_c are the respective Young's moduli of the substrate and cell (5); see the Supporting Material for additional parameters used. To see this figure in color, go online.

expansion modulus, κ_c, here we wish to explicitly represent myosin activity in our expression for the force and to demonstrate how the augmentation of actomyosin force in time may affect the evolution of cell area and total force during spreading. Generalizing Eq. 2, we write

$$f/h = 2\,\kappa_c\,(R-R_0)/R_0 + \xi_c\,\dot{R}/R_0 - P(t), \qquad (6)$$

where $P(t)$ represents the radial myosin stress; the negative sign is here to indicate that the contractile activity of myosin ($P(t) < 0$) generates (positive) elastic tension in the cytoskeleton. To focus on the new effects arising from the polarization response of myosin contraction, we treat R_0 as a constant. Based on a variety of theoretical and experimental studies indicating that myosin activity responds to the local stress in the cytoskeleton (8), we write the following phenomenological relaxation response to account for its early-time dynamics (see Nisenholz et al. (9) for a more detailed treatment):

$$\tau_p\dot{P} = -2\kappa_c\alpha(R-R_0)/R_0 - [P-P_0]. \qquad (7)$$

Here, τ_p, represents the timescale of the polarization response (namely, of the increase in the magnitude of the actomyosin stress, $P(t)$); α reflects the susceptibility of the acto-myosin dipolar stress, P, to the evolving elastic stress; and P_0, is the initial acto-myosin dipolar stress. In the steady state,

$$\dot{P} = 0 \text{ and } P_{ss} - P_0 = -2\alpha\kappa_c(R-R_0)/R_0.$$

In cases where myosin polarization response is sufficiently strong (large α), and fast (τ_p small compared to overall spreading time), myosin forces would dominate the overall force, f, at early times, and one expects to find a characteristic acceleration of f in time. Such behavior is observed in Fig. 1 (*green fit*). Hence myosin polarization provides a second mechanism that may contribute to the apparent delay in force generation relative to area increase. However, we note that our data fitting should not be taken as a quantitative measurement of τ_p and α, inasmuch as all three mechanisms (I–III) might be operating simultaneously during spreading.

III: nonlinear elasticity of the cytoskeleton

A third mechanism that may inevitably contribute to the delay in force production is strain-stiffening of the cytoskeleton (9,10). This is particularly expected in cases where initial spreading occurs with a relatively soft cytoskeleton, and consequently only weak tensile stresses are generated at early spreading. Strain-stiffening causes a delayed increase in cellular force. Replacing the Hookean term in Eq. 2 by an exponential strain-stiffening term (10), one writes

$$f/h = (2\kappa_c/\lambda)\left[e^{\lambda(R-R_0)/R_0} - 1\right] + \xi_c\,\dot{R}/R_0. \qquad (8)$$

Combining this equation with Eq. 3 reveals an analytically solvable equation for cell-spreading dynamics (5). The fit to experimental data is shown in Fig. 1 (*blue curves*).

This mechanism is somewhat similar in effect to a slow assembly of the lamellar network, as considered in (I) above. However, the origin of the delay in force generation is different. In the current scenario, the nonlinear dependence of $f(t)$ on $R(t)$ arises from the passive constitutive relation of the cytoskeleton. In the assembly mechanism (I) and acto-myosin polarization mechanism (II), the apparent nonlinearity of $f(R)$ is a consequence of the different dynamics of $R(t)$ and $f(t)$ but the cytoskeletal constitutive relation is linear. Because R and f cease to evolve in the steady state, systematic measurements of their steady-state values may shed light on the actual constitutive relation relevant for spreading, as demonstrated in Fig. 2. The dashed lines indicate the end-points of spreading on differently rigid substrates. For an intrinsically nonlinear cytoskeleton, all end-points must fall on a nonlinear curve that represents the cytoskeleton constitutive relation. In contrast, a linear relation between f_{ss} and R_{ss} is expected for (I) and (II) above. A scatter plot of cell area and force in the steady state is provided in Fig. S3; the overall trend is consistent with previous reports (4), which have suggested that F_{ss} scales linearly with A_{ss}. However, because the R^2 value in these plots is rather small, additional experiments would need to be carried out to reconcile to what extent the cytoskeleton behaves in a linear fashion during spreading.

SUPPORTING MATERIAL

Five supporting information sections, three figures, and two tables are available at http://www.biophysj.org/biophysj/supplemental/S0006-3495(14)01136-9.

AUTHOR CONTRIBUTIONS

Yifat Brill-Karniely and Noam Nisenholz contributed equally to this article.

ACKNOWLEDGMENTS

We are grateful to the Israel Science Foundation (grant No. 1396/09) and the Niedersachsen, German-Israeli Lower Saxony Cooperation, for their support.

REFERENCES and FOOTNOTES

1. Giannone, G., B. J. Dubin-Thaler, …, M. P. Sheetz. 2004. Periodic lamellipodial contractions correlate with rearward actin waves. *Cell.* 116:431–443.
2. Schwarz, U. S., and M. L. Gardel. 2012. United we stand: integrating the actin cytoskeleton and cell-matrix adhesions in cellular mechanotransduction. *J. Cell Sci.* 125:3051–3060.
3. Dubin-Thaler, B. J., J. M. Hofman, …, M. P. Sheetz. 2008. Quantification of cell edge velocities and traction forces reveals distinct motility modules during cell spreading. *PLoS ONE.* 3:e3735.
4. Reinhart-King, C. A., M. Dembo, and D. A. Hammer. 2005. The dynamics and mechanics of endothelial cell spreading. *Biophys. J.* 89:676–689.
5. Nisenholz, N., K. Rajendran, …, A. Zemel. 2014. Active mechanics and dynamics of cell spreading on elastic substrates. *Soft Matter.* 10: 7234–7246.
6. Fouchard, J., C. Bimbard, …, A. Asnacios. 2014. Three-dimensional cell body shape dictates the onset of traction force generation and growth of focal adhesions. *Proc. Natl. Acad. Sci. USA.* 111:13075–13080.
7. Walcott, S., and S. X. Sun. 2010. A mechanical model of actin stress fiber formation and substrate elasticity sensing in adherent cells. *Proc. Natl. Acad. Sci. USA.* 107:7757–7762.
8. Zemel, A., R. De, and S. A. Safran. 2011. Mechanical consequences of cellular force generation. *Curr. Opin. Solid State Mater. Sci.* 15: 169–176.
9. Nisenholz, N., M. Botton, and A. Zemel. 2014. Early-time dynamics of actomyosin polarization in cells of confined shape in elastic matrices. *Soft Matter.* 10:2453–2462.
10. Kollmannsberger, P., C. T. Mierke, and B. Fabry. 2011. Nonlinear viscoelasticity of adherent cells is controlled by cytoskeletal tension. *Soft Matter.* 7:3127–3132.

Supplementary Information

Dynamics of cell size and force during *spreading*

Yifat Brill-Karniely[1], Noam Nisenholz[1], Kavitha Rajendran[2], Quynh Dang[2], Ramaswamy Krishnan[2], and Assaf Zemel[1],*

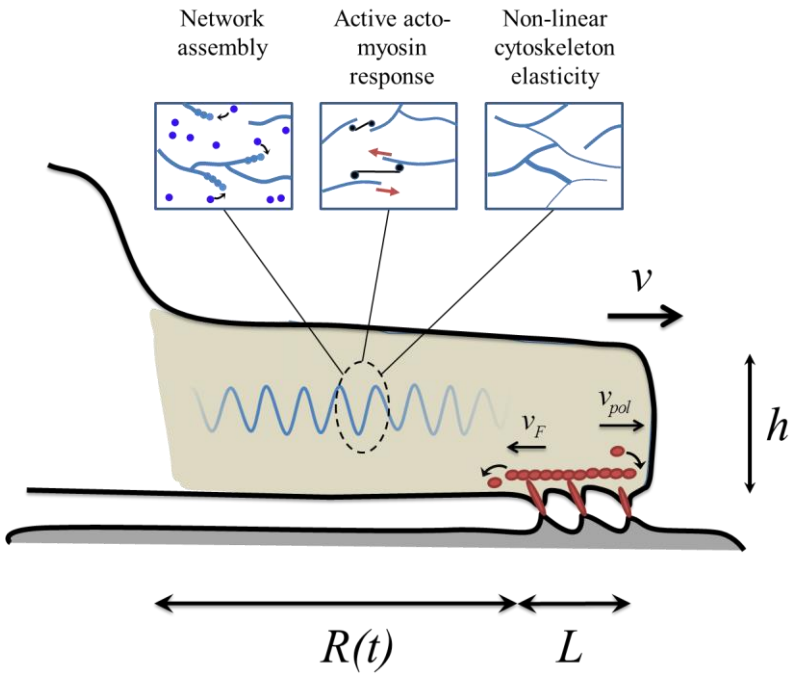

Figure S1: Schematic illustration of major elements of the model. The cell is modeled as a circular disc of radius *R(t)* and thickness *h* that is adhered to the substrate along a narrow rim, $L \ll R(t)$ that is assumed to be constant during spreading. Actin polymerization (red circles) at the cell front provides the driving force for cell spreading. Experiments suggest that the radial polymerization speed, v_{pol}, is constant during spreading. In contrast, the retrograde flow, $v_F(t)$, increases in the course of spreading while the radial extension speed, $v(t) = dR(t)/dt$, decelerates with time (1). This is explained here by the rise in elastic tension in the cytoskeleton. The shaded spring in the cell center is there to represent the underlying viscoelastic response of the cell (including the cytoskeleton and the membrane). Three models are presented to account for the non-linear coupling between cell size and force during spreading; those are shown with the three cartoons above. Left, middle and right panels illustrates the network assembly model, actomyosin polarization model and the non-linear elastic model, respectively.

1. Materials and Methods

Combined, time-resolved force and area measurements in cultured human pulmonary artery endothelial cells (HPAECs)

Preparation of gel-substrates: Cells (Lonza,cat#CC-2530) were detached with 0.25% Trypsin- EDTA (1x) (Life Technologies, cat #25200-056) from a standard cell culture flask and re-suspended in growth medium (EGM2 bulletkits, cat # CC-3162, Lonza Inc.) supplemented with 10% fetal bovine serum (cat#45000-736, VWR International). The medium containing cells was then added to the surface of 26kPa stiff polyacrylamide gel substrates. The substrates were prepared within 35mm glass bottom dishes (Mattek, USA) as has been previously described (2) with a few modifications. Briefly, a small volume of an acrylamide-Bisacrylamide mixture was dissolved in ultrapure water containing 7.5% acylamide, 0.3% Bisacrylamide, 0.5% ammonia persulfate, and 0.05% TEMED (Bio-Rad, Hercules, CA) and polymerized between glass coverslips to yield gels that were ~100 μm thick. The polymerized gel surfaces were activated using Sulfosuccinimidyl-6-[4-azido-2-nitrophenylamino] hexanoate (Sulfo-SANPAH; Pierce, Rockford, IL) and conjugated with sulfate-modified fluorescent latex nanospheres (diameter = 200 nm, F8848, Life Technologies) by delivering a bead suspension on top of the gels for 20 minutes (3). The bead solution was carefully removed to discard any suspended or unattached beads, replaced with type I Collagen dissolved in PBS solution (0.1 mg/ml; cat#5505-B, Advanced Biomatrix) and stored overnight at 4°C. The bead binding step was repeated on the following day. The gels were then washed, hydrated with PBS, and stored at 4°C until the day of the experiment.

Cell-spreading measurements: All measurements were performed in a microscope chamber (37^0C and 5% CO2) using an inverted fluorescence microscope (DMI 6000B, Leica Inc). Phase contrast images of cells were obtained together with fluorescent images of nanospheres. From the phase contrast images, by manually tracing cell contours, we calculated the cell spreading area. From the fluorescent nanosphere images, by comparing images during cell spreading with the same region of the gel after cell detachment from the substrate, we calculated the cell-exerted displacement field. The displacements were calculated through cross-correlation using

the fast fourier transform method in Matlab. From knowledge of the displacement field together with the previously determined gel elastic modulus (26 kPa), we computed the cell-generated forces by solving the inverse Boussinesq solution using the well-established procedure of Fourier transform traction microscopy (2). During its implementation, we minimized any experimental artifacts that may have arisen during the measurements of displacements through the constrained traction method, where tractions outside the boundary of the cell are set to be zero. From the traction map, we calculated total force over the cell, *F*, by summing the absolute magnitude. Next, we determined the traction density as $f=F/(2\pi R)$. These calculations were performed from experimental measurements obtained every five minutes for the total duration of approximately an hour.

2. **Effect of cell volume on spreading dynamics**

It is generally expected that cells of larger volume and larger cytoskeleton mass would show a longer period in which the assembly of the cytoskeleton network at the cell basis accompanies spreading. According to our elastic picture, this process changes the effective "rest-length'' of the cytoskeleton and therefore modulates the dynamics of force generation during spreading. To the best of our knowledge, it is unknown how *cell volume* alters the dynamics and mechanics of spreading. Thus, in this section we examine this issue theoretically. In comparing cells of different volumes we assume that the concentration of suspended cytoskeletal material, c(0), is fixed. In addition, the initial projected cell radius, $R(0)$, is assumed to scale with the cell volume and to be equal to the stress-free radius, $R_0(0)$, such that in the onset of spreading, $R(0) = R_0(0) = \beta V^{1/3}$; where β is a proportionality constant that can be obtained by the fit to experimental data. Eqs. 4 and 5 provide a simple kinetic model for the growth-dynamics of the stress-free area of the lamellar cytoskeleton $A_0(t) = \pi R_0^2(t)$ at the cell basis. Accordingly, the larger the cell volume, and consequently also A_0, the faster is the assembly rate since the number of available binding sites is larger. As a result, the cell may spread by assembling the lamellar cytoskeleton, and yet without generating elastic stresses in the cytoskeleton. This is shown for example by the red curves in Fig. S2. Panels a. and b. show the evolution of cell radius and

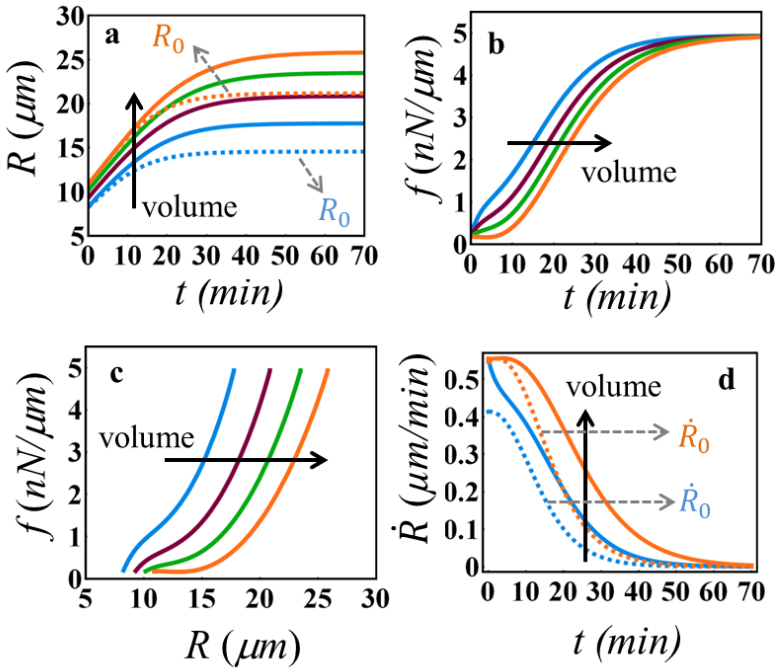

Figure S2: Effects of cell volume on spreading dynamics and mechanics. Panels a and b exhibit the evolution of cell radius and force respectively. Dashed lines in (a) is the stress-free radius as calculated analytically from Eqs. 4 and 5. Panel c. shows a parametric plot of the radial cell force as a function of cell radius. Panel (d) presents the radial spreading speed, $\dot{R}(t)$, along with the radial assembly speed, $\dot{R}_0(t)$ for the largest (orange) and smallest (light blue) cells. Parameters used in the calculation are: *V* (μm^3)=*2200* (light blue), *3150* (purple), *4100* (green), *5050* (orange), *h=1 μm*, $\rho=1.1\cdot10^7$ *molec/μm*^{2}, *c(0)=3.8 mM*, v_{pol}*=0.58 μm/min*, κ_c*=11* kPa, ξ_c*=1.67* kPa·*min*, ξ_s *=8.4* kPa·*min*, δ*=26.4 (M·min)*$^{-1}$.

force, respectively. So long as the radial assembly speed is equal to the spreading velocity, $v = \dot{R} \approx \dot{R}_0$, no tension is developed in the cell. The elastic phase begins once the available suspended material for lamellar assembly diminishes and consequently further spreading is associated with stress generation.

In cells of smaller volume (e.g., light blue), the assembly rate is slower due to the smaller number of binding sites on the smaller 2D network area. However, because the polymerization speed, v_{pol}, is likely to be similar (since it is dictated by similar G-actin concentration), the spreading speed $v = \dot{R}$ can exceed the assembly-growth speed $\dot{R}_0$ and as a result the cell may develop tension already at early-times. The comparison between $\dot{R}_0(t)$ and $\dot{R}(t)$ is shown in panel (d) for two cells that only differ in volume. While for both cell cases, $\dot{R}(0) \approx v_{pol}$ since no elastic tension has yet been generated (and the viscous force is relatively small), $\dot{R}_0(t)$ is lower for the

smaller cell and consequently stresses develop more quickly in the onset of spreading. The effects of these different dynamics on the $f(t)$ versus $R(t)$ curve is shown in panel c. The apparent non-linearity of $f(R)$ is seen to be more pronounced the larger the cell is.

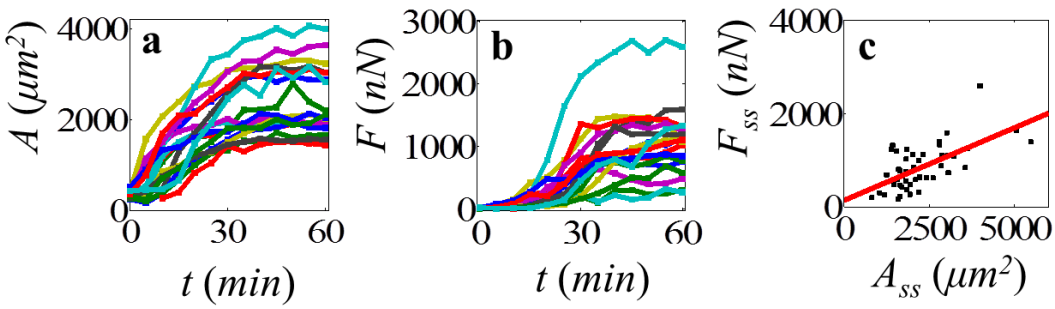

Figure S3: Evolution of cell area and total force during spreading. Panels a. and b. show the respective spreading data for 18 representative cells in our collection. Panel c. is a scatter plot of the *steady-state* force and area, collecting the end-points from our entire collection of cells (47 cells). Red line is a linear fit (slope=0.31 kPa, R^2=0.4).

3. Data for total cell force and area

Fig. S3 shows measured data of the evolution of cell area, $A(t)$, and total cell force, $F(t)$, for individual cells in our collection. These are related to the temporal traction density, f, and cell radius via: $F \approx 2\pi R\, f$ and $A \approx \pi R^2$. Panel c. provides a scatter plot of the steady-state force, F_{ss} as function of the steady-state area of cells, A_{ss}. The seemingly linear dependence between F_{ss} and A_{ss} suggests that also f_{ss}~R_{ss}; yet note the small R^2 value. Manipulating the data to plot f_{ss} as function of R_{ss}directly, increases the relative noise and the corresponding R^2 value reduces to 0.06. Nevertheless, we note the apparent difference in the behavior of the steady-state dependence of F_{ss} on A_{ss}, Fig. S3.c, and the profound non-linear dependence of the temporal force $f(t)$ on $R(t)$, shown in Fig.1c. A linear dependence of F_{ss} on A_{ss} may indicate that the cytoskeleton behaves in a linear fashion during spreading and the apparent non-linearity of the $f(R)$ curve would then be explained by the different dynamics of cell area and force as explained with models (i) and (ii) in the manuscript. Nevertheless, since the R^2=0.4 is rather low in panel c. we are unable to reach any conclusion about this issue in the current manuscript.

Table S1. Parameters used in Figure 1.

Parameter	Notation	Network assembly	Actomyosin polarization	Non-linear	Refs (in SI)
Initial lamella radius*	*R(0) (μm)*	11.2	10.3	10.8	-
Average lamella height	*h (μm)*	1.7	1	1	4,5
Cell volume	*V (μm^3)*	4500	-	-	-
Surface density of lamellar network	*ρ (molec/μm^2)*	$1.85 \cdot 10^7$	-	-	6
Assembly rate constant	*δ (M·min)$^{-1}$*	9.96	-	-	-
Initial concentration of suspended cytoskeleton constituents (based on actin)	*c(0) (mM)*	9.2	-	-	6
Radial actin polymerization speed	*v_{pol} (μm/min)*	0.59	0.68	0.63	1
Effective cytoskeletal rigidity	*κ_c (*kPa*)*	10	0.07	0.13	8
Lamella viscosity coefficient	*ξ_c (*kPa·*min)*	1	0.07	3.58	9
Cell-substrate friction coefficient	*ξ_s (nN·min/μm^2)*	8.3	6.4	7.2	-
Stress-stiffening factor	*λ*	-	-	2.75	7
Actomyosin susceptibility	*α*	-	22	-	-
Actomyosin polarization response time	*τ_p (min)*	-	15	-	-

* $R(0) = R_0$ in the polarization and non-linear models and $R(0) = R_0(0)$ in the assembly model.

4. Data Fitting in Figure 1

Table S1 lists the parameters obtained from fitting the three models to our experimental data. The right most column provides references (listed at the bottom of this document) for comparison for few of the fitted parameters. The order of magnitude of the phenomenological surface density parameter, ρ, and initial concentration of suspended constituents, *c(0)* is consistent with the size ($v = h/\rho \sim 10^{-7}\mu m^3$) and bulk-concentration of actin monomers (Ref. 6) which is the main polymer in the lamellar network. The cytoskeleton viscosity, $\xi_c = 1\ kPa\ min$ is

estimated based on the measurements in Ref. 9 below. Since the number of fitting parameters is large, (between 6-7) and more importantly, since it is very likely that the three mechanisms operate simultaneously the values we obtain by these fits *should not* be considered as quantitative estimates of these parameters. Rather, the purpose of the fits shown in Fig.1 is to demonstrate that all three models may separately capture the *qualitative* behavior of cell size and force during spreading and hence to contribute to the observed phenomena.

5. Comments and parameters for Fig. 2

Fig. 2 highlights the difference between the temporal dependence of $f(t)$ on $R(t)$ (solid lines) and the corresponding dependency of the steady-state values of f_{ss} and R_{ss} (dashed lines). While the relation between $f(t)$ and $R(t)$ reflects the various dynamical processes that take place in the cytoskeleton during spreading (such as network assembly and actomyosin polarization), the dependence of f_{ss} on R_{ss} (and equivalently of F_{ss} on A_{ss}, Fig. S2) reflects the underlying (passive) constitutive relation of the cytoskeleton. Different curves were plotted for various values of the substrate rigidity. A relatively high viscosity constant, ξ_c *=45* kPa·min was used in order to visually separate the different curves; this also required adjustment of the network assembly rate constant, δ, to keep the early-time force comparable to the two other models. The values of κ_c were adjusted in the three models to obtain the same level of overall strain $(R_{ss} - R_0)/R_0$ since both the acto-myosin polarization model and the nonlinear elasticity model possess different stiffening mechanisms of the cytoskeleton, one via the polarizability factor, $\propto$, the other via the stiffening factor λ. Finally, throughout, we used $P_0 = 0$ implying that $P(t) - P_0 = P(t)$ measures the strengthening of the acto-myosin dipolar stress. The basal level of myosin contraction is then implicitly represented in the value of the cytoskeleton rigidity, κ_c. The parameters used in Fig. 2 are listed in Table S2.

Table S2. Parameters used in Figure 2

Parameter	Notation	Network assembly	Actomyosin polarization	Non-linear
Initial lamella radius*	$R(0)\ (\mu m)$	10	10	10
Average lamella height	$h\ (\mu m)$	1	1	1
Cell volume	$V\ (\mu m^3)$	4500	-	-
Surface density of lamellar network	$\rho\ (molec/\mu m^2)$	$1.85 \cdot 10^7$	-	-
Assembly rate constant	$\delta\ (M \cdot min)^{-1}$	55.8	-	-
Initial concentration of suspended cytoskeleton constituents (based on actin)	$c(0)\ (mM)$	9.3	-	-
Radial actin polymerization speed	$v_{pol}\ (\mu m/min)$	0.8	0.8	0.8
Effective cytoskeletal rigidity	κ_c (kPa)	10	1.4	1.9
Lamella viscosity coefficient	ξ_c (kPa·min)	45	45	45
Cell-substrate friction coefficient	$\xi_s^{max}\ (nN \cdot min/\mu m^2)$	10	10	10
Stress-stiffening factor	λ	-	-	2.75
Acto-myosin susceptibility	α	-	3	-
Actomyosin polarization response time	$\tau_p\ (min)$	-	2	-

6. References

1. Giannone, G., B. J. Dubin-Thaler, H.-G. D¨obereiner, N. Kieffer, A. R. Bresnick, and M. P. Sheetz, 2004. Periodic lamellipodial contractions correlate with rearward actin waves. *Cell* 116:431–43.
2. Butler, J. P., Toli´c-Nørrelykke, I. M., Fabry, B. & Fredberg, J. J. Traction fields, moments, and strain energy that cells exerton their surroundings. *American Journal of Physiology-Cell Physiology* 282, C595–C605 (2002).
3. Marinković, A., Mih, J. D., Park, J. A., Liu, F., & Tschumperlin, D. J. (2012). Improved throughput traction microscopy reveals pivotal role for matrix stiffnes in fibroblast contractility and TGF-β responsiveness. *American Journal of Physiology-Lung Cellular and Molecular Physiology*, *303*(3), L169-L180.
4. Pang, K. M., E. Lee, and D. a. Knecht, 1998. Use of a fusion protein between GFP and an actin-binding domain to visualize transient filamentous-actin structures. *Curr. Biol.* 8:405–8.
5. Fardin, M., O. Rossier, P. Rangamani, P. Avigan, N. Gauthier, W. Vonnegut, A. Mathur, J. Hone, R. Iyengar, and M. Sheetz, 2010. Cell spreading as a hydrodynamic process. *Soft Matt.* 6:4788–4799.
6. Lodish, H., Berk, A., Kaiser, CA., Krieger, M., Scott, MP., Bretcher, A., Ploech, H. and Matsudaira, P, 2012. Molecular Cell Biology 7th edition, Macmillan Higher Education, Aug 1, 2012 - Science.
7. Kollmannsberger, P., Mierke, C. T. & Fabry, B. Nonlinear viscoelasticity of adherent cells is controlled by cytoskeletal tension.*Soft Matter* 7, 3127–3132 (2011).
8. Rodriguez, Marita L., Patrick J. McGarry, and Nathan J. Sniadecki. "Review on cell mechanics: experimental and modeling approaches." Applied Mechanics Reviews 65.6 (2013): 060801.
9. Bausch, Andreas R., Winfried Möller, and Erich Sackmann. "Measurement of local viscoelasticity and forces in living cells by magnetic tweezers." Biophysical journal 76.1 (1999): 573-579.